SCISPACE
formerly Typeset

Open access • Journal Article • DOI:10.13182/FST00-A141

A General Computational Approach for Magnetohydrodynamic Flows Using the CFX Code: Buoyant Flow Through a Vertical Square Channel — Source link

Ivan Di Piazza, Leo Bühler

Institutions: University of Palermo

Published on: 01 Sep 2000 - Fusion Technology (American Nuclear Society)

Topics: Magnetohydrodynamic drive, Magnetohydrodynamics, Boundary value problem, Flow conditioning and Magnetic field

Related papers:

- Laminar buoyant magnetohydrodynamic flow in vertical rectangular ducts
- Magnetofluiddynamics in Channels and Containers
- Numerical simulations of buoyant magnetohydrodynamic flows using the CFX code
- Magnetohydrodynamic flow in rectangular ducts
- Monotone Scheme and Boundary Conditions for Finite Volume Simulation of Magnetohydrodynamic Internal Flows at High Hartmann Number

Share this paper:

View more about this paper here: https://typeset.io/papers/a-general-computational-approach-for-magnetohydrodynamic-1f30lxi64a

A GENERAL COMPUTATIONAL APPROACH FOR MAGNETOHYDRODYNAMIC FLOWS USING THE CFX CODE: BUOYANT FLOW THROUGH A VERTICAL SQUARE CHANNEL

BLANKET ENGINEERING

KEYWORDS: *magnetohydrodynamic flow, buoyant flow, CFX code*

IVAN DI PIAZZA* *Dipartimento di Ingegneria Nucleare*
Università degli Studi di Palermo, Viale delle Scienze, 90128 Palermo, Italy

LEO BÜHLER *Forschungszentrum Karlsruhe*
Institut für Kern -und Energietechnik, Postfach 3640, D-76021 Karlsruhe, Germany

Received September 3, 1999
Accepted for Publication December 20, 1999

The buoyancy-driven magnetoconvection in the cross section of an infinitely long vertical square duct is investigated numerically using the CFX code package. The implementation of a magnetohydrodynamic (MHD) problem in CFX is discussed, with particular reference to the Lorentz forces and the electric potential boundary conditions for arbitrary electrical conductivity of the walls. The method proposed is general and applies to arbitrary geometries with an arbitrary orientation of the magnetic field. Results for fully developed flow under various thermal boundary conditions are compared with asymptotic analytical solutions. The comparison shows that the asymptotic analysis is confirmed for highly conducting walls as high velocity jets occur at the side walls. For weakly conducting walls, the side layers become more conducting than the side walls, and strong electric currents flow within these layers parallel to the magnetic field. As a consequence, the velocity jets are suppressed, and the core solution is only corrected by the viscous forces near the wall. The implementation of MHD in CFX is achieved.

I. INTRODUCTION

Two different schemes have been proposed in recent years for the liquid-metal breeding blankets of fusion reactors: In one of them the coolant coincides with the liquid breeder itself (self-cooled concept), while in the other the heat flux is removed by separated coolant devices (i.e., water-cooled concept). A comparison of these two concepts has been performed within the European projects.[1] In the self-cooled concept, high velocities are required to remove heat; thus, the flow must be strongly forced, which is expressed by relatively large pressure losses induced by magnetohydrodynamic (MHD) effects. Under these conditions, the buoyancy effects are negligible. Of course, this is not the case for separately cooled devices, where a weak forced flow is required only for tritium extraction, and relevant temperature gradients occur; therefore, the flow is mainly buoyancy driven.

Within this separately cooled concept, the buoyant fully developed flow across a vertical square channel under the influence of a magnetic field is investigated numerically. The walls are supposed to be electrically conducting and thin, and the influence of the wall conductivity on the flow pattern is studied. Various thermal conditions are examined, i.e., the differentially heated and the internally heated cases. The implementation of MHD in the CFX code package[2] for arbitrary configurations is described with particular attention to the Lorentz forces, the potential equation, and the electrical boundary conditions.

For the same geometry, an asymptotic analysis[3] has been developed for large Hartmann numbers and highly conducting walls parallel to the magnetic field, the so-called side walls. It is shown here that these analytical results are confirmed by numerical simulations for the highly conducting walls. In particular, high velocity jets in the side layers are correctly predicted. For low values of wall conductivity, strong electric currents parallel to the side walls appear in the side layers, and the numerical simulations show that the velocity jets are suppressed.

*E-mail: ivandp@din.din.unipa.it

Moreover, the ability of CFX in predicting actual MHD flows is proved.

In the past, several authors have solved numerically buoyant MHD flow problems.[4] Others solved pressure-driven MHD flows.[5,6] The common restrictions of all these analyses is that they are limited to very special geometries, hardly met in engineering piping systems. The use of CFX in MHD modeling offers the possibility to perform inertial numerical simulations for relevant duct shapes and complex geometries.

II. FORMULATION

The problem presented here is the MHD buoyancy-driven flow in a vertical square duct. Figure 1 shows a sketch of the geometry. The magnetic field $\mathbf{B} = B\hat{\mathbf{y}}$ is parallel to a pair of walls and orthogonal to the other one. The walls normal to the magnetic field are called the Hartmann walls. In the boundary layers close to these walls, the velocity profile is basically determined from a balance between Lorentz and viscous forces, and the thickness of these layers scales as $\delta_H \sim M^{-1}$, where M is the Hartmann number, which is better defined later in the section. The walls parallel to the magnetic field direction are called the side walls, and the boundary layers adjacent to these walls, the side layers. Their thickness δ_s scales as $\delta_s \sim M^{-1/2}$. The temperature gradient is supposed to be directed along $\hat{\mathbf{z}}$, and thus orthogonal to the magnetic field direction $\hat{\mathbf{y}}$.

Under the assumption of a low magnetic Reynolds number, the induced magnetic field is negligible with respect to the applied field $\mathbf{B}$. Such an inductionless flow

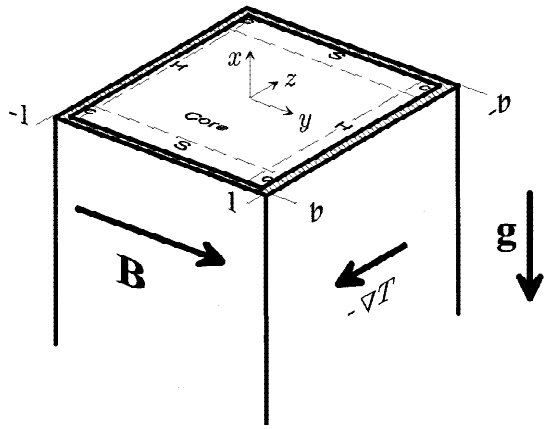

Fig. 1. Sketch of the geometry of the channel. The gravity field is in the axis direction, and the magnetic field is parallel to one pair of walls and orthogonal to the others. The temperature gradient is in the $\hat{\mathbf{z}}$ diection, orthogonal to the magnetic field.

is governed by the momentum equation with the Boussinesq approximation for the buoyancy term,

$$\frac{\mathrm{Gr}}{M^4}\left[\frac{\partial \mathbf{v}}{\partial t} + (\mathbf{v}\cdot\nabla)\mathbf{v}\right] = -\nabla p + \frac{1}{M^2}\nabla^2\mathbf{v} + \mathbf{j}\times\hat{\mathbf{y}} + T\hat{\mathbf{x}} \ , \tag{1}$$

and the continuity equation,

$$\nabla\cdot\mathbf{v} = 0 \ . \tag{2}$$

Gr is the Grashof number, which expresses the square of the ratio of buoyancy and viscous forces, defined as

$$\mathrm{Gr} = g\beta\Delta T L^3/\nu^2 \ , \tag{3}$$

where β is the thermal expansion coefficient of the fluid. The velocity vector $\mathbf{v} = (u,v,w)$ and the current density $\mathbf{j}$ are scaled respectively by $v_0 = \nu/L\cdot\mathrm{Gr}/M^2$ and $j_0 = \sigma v_0 B$, where L is a characteristic length scale, ν is the kinematic viscosity, and σ is the electrical conductivity of the fluid. The dimensionless pressure p is the difference between the local and the hydrostatic pressure, scaled by Lj_0B. The dimensionless temperature T is the difference between the local temperature and a reference value T_0, scaled by a characteristic temperature difference ΔT. The square of the Hartmann number M is the ratio of electromagnetic to viscous forces, and it can be defined as

$$M = LB\sqrt{\sigma/(\rho\nu)} \ , \tag{4}$$

where ρ is the density of the fluid.

These scales are particularly appropriate for strong magnetic fields, and one can observe that the velocity scale is the diffusion scale ν/L times the quantity Gr/M^2; this quantity is actually the ratio of buoyant to electromagnetic forces and takes into account the damping effect of the magnetic field. The quantity M^4/Gr is the square of the Lykoudis number or corresponds to an interaction parameter. It represents the ratio of the electromagnetic and the inertial forces. The current is given by Ohm's law

$$\mathbf{j} = -\nabla\phi + \mathbf{v}\times\hat{\mathbf{y}} \ , \tag{5}$$

together with the conservation of the electric charge

$$\nabla\cdot\mathbf{j} = 0 \ . \tag{6}$$

The electrical potential ϕ is scaled by Lv_0B.

The temperature is governed by the energy balance:

$$\mathrm{Pe}\left[\frac{\partial T}{\partial t} + (\mathbf{v}\cdot\nabla)T\right] = \nabla^2 T + Q \ , \tag{7}$$

where $\mathrm{Pe} = \mathrm{Pr}\,\mathrm{Gr}/M^2$ is the Péclet number, and Q represents the volumetric power density scaled by $\lambda\Delta T/L^2$, with the thermal conductivity λ. Pr represents the Prandtl number defined as the ratio of the kinematic viscosity to the thermal diffusivity of the fluid.

The boundary conditions for the velocity are the no-slip conditions at the walls, while the thermal boundary conditions are $\mathbf{n}\cdot\nabla T = const.$ at the Hartmann walls, and $T = const.$ or $\mathbf{n}\cdot\nabla T = -q_w$ at the side walls, where $\mathbf{n}$ is the inward unity vector normal to the wall.

The electrical boundary condition is the thin wall condition[7]

$$\mathbf{j}\cdot\mathbf{n} = c_w \nabla_w^2 \phi \ , \tag{8}$$

which expresses the conservation of the electric charge in the plane of the wall. The condition is integrated across the wall thickness, and the constant c_w is called the wall conductance ratio $c_w = \sigma_w t$, where the conductivity of the wall is scaled by the fluid conductivity and the dimensionless thickness of the wall t is assumed to be small $t \ll 1$.

For sufficiently long ducts, the flow is fully developed far from the ends; inertia does not play any role, and the left sides of Eqs. (1) and (7) vanish. Therefore, the solution is no more dependent on Gr and Pe, and the only relevant parameters entering the equations are M and c_w. The problem is actually two-dimensional in the plane perpendicular to the axis of the duct.

Under these conditions, an asymptotic analysis[3] has been performed assuming a large Hartmann number and a conductivity c_s of the side walls such that

$$c_s \gg M^{-1/2} \ . \tag{9}$$

This condition implies that the side walls must be much better conducting than the side layers. Therefore, the currents are supposed to cross entirely the side layers and close through the walls only.

III. DESCRIPTION OF AN MHD PROBLEM IN CFX

The CFX code[2] is a commercial package for fluid dynamic calculations, based on the finite volume technique and the SIMPLE family algorithms for the pressure-velocity coupling. It is, in principle, a very powerful and flexible code, for arbitrary geometries with orthogonal, polar, or body-fitted coordinates, turbulence models, chemical reactions, two-phase flow, etc.

Unfortunately, MHD is not available at all as a simple option of the code, and an MHD problem must be properly described within the code by the user himself. The equations describing the fluid behavior in CFX are the following:

The momentum equation

$$\frac{\partial \bar{\rho}\bar{\mathbf{v}}}{\partial \bar{t}} + \bar{\rho}(\bar{\mathbf{v}}\cdot\nabla)\bar{\mathbf{v}} = -\nabla\bar{p} + \nabla\bar{\mu}\nabla\bar{\mathbf{v}} + S_m \ , \tag{10}$$

the continuity equation

$$\nabla\cdot\bar{\mathbf{v}} = 0 \ , \tag{11}$$

and the temperature equation

$$\frac{\partial \bar{\rho}\bar{c}_p \overline{T}}{\partial \bar{t}} + \nabla\cdot(\bar{\mathbf{v}}\bar{\rho}\bar{c}_p \overline{T}) = \nabla\bar{\lambda}\nabla\overline{T} + S_{\overline{T}} \ , \tag{12}$$

where the overbar is used to indicate the internal CFX variables. In addition to this set of equations, the transport of an arbitrary scalar is described as

$$\frac{\partial \bar{\rho}\bar{\theta}}{\partial \bar{t}} + \nabla\cdot(\bar{\mathbf{v}}\bar{\rho}\bar{\theta}) = \nabla\Gamma_{\bar{\theta}}\nabla\bar{\theta} + S_{\bar{\theta}} \ . \tag{13}$$

In the following, CFX will be applied to the nondimensional system Eqs. (1) through (8). The coefficients with an overbar necessary for a CFX input are therefore chosen as

$$\bar{\rho} = \frac{\mathrm{Gr}}{M^4} \ , \quad \bar{\mu} = \frac{1}{M^2} \ , \quad \bar{\lambda} = 1 \ , \quad \bar{c}_p = 1 \ . \tag{14}$$

Such a choice allows an interpretation of the CFX-variables $\bar{\mathbf{v}}$, $\bar{p}$, $\overline{T}$, and $\bar{\theta}$ as the dimensionless velocity vector $\mathbf{v}$, the pressure p, the electrical potential ϕ, and the temperature T, respectively. The reason why $\overline{T}$ is preferred to $\bar{\theta}$ as a representation of the electrical potential is that Eq. (12) allows more general boundary conditions than Eq. (13) does.

Basically, there are three points that have to be implemented in the external routines to the code. The source term S_m in the Navier-Stokes equations includes buoyancy $\bar{\theta}\,\hat{\mathbf{x}}$ and Lorentz force

$$\mathbf{j}\times\hat{\mathbf{y}} = -\nabla\phi\times\hat{\mathbf{y}} + (\mathbf{v}\times\hat{\mathbf{y}})\times\hat{\mathbf{y}} \ , \tag{15}$$

which can be split in a potential gradient component $-\nabla\phi\times\hat{\mathbf{y}}$, and another component $(\mathbf{v}\times\hat{\mathbf{y}})\times\hat{\mathbf{y}} = -\mathbf{v}_\perp$ similar to a drag term that is acting in the plane perpendicular to the magnetic field. Therefore, the gradient of ϕ must be evaluated numerically as part of the source term in the momentum equation.

From Eqs. (5) and (6), an equation for the scalar electrical potential can easily be derived

$$-\nabla^2\phi = -(\nabla\times\mathbf{v})\cdot\hat{\mathbf{y}} = S_{\overline{T}} \ . \tag{16}$$

Using this equation, the currents are eliminated from the problem. It can be recognized that Eq. (16) has the form of a diffusion transport equation, the source term being the component of vorticity along the magnetic field direction. Thus, it is possible to describe this equation in CFX as a scalar transport equation, with no convection, and a source term evaluated by the spatial derivatives of velocity.

The electrical boundary conditions Eq. (8) combined with Ohm's law Eq. (5) evaluated at the wall lead to

$$-\mathbf{n}\cdot\nabla\phi = c_w\nabla_w^2\phi \ . \tag{17}$$

The potential equation Eq. (16) in the fluid, together with the boundary condition Eq. (17), is the electrical problem analogous to a heat transfer problem in a medium at rest, surrounded by a thin sheet of different conductivity. Such problems can be solved using existing routines in CFX in combination with the "no convection" option, when the CFX-temperature $\bar{T}$ is interpreted as the electrical potential ϕ in the MHD problem under consideration. Then the CFX-heat fluxes represent simply the electric currents. This is valid at the walls, where the velocity vanishes and the current simply becomes $\mathbf{j} = -\nabla\phi$. However, the CFX-heat fluxes in the fluid do not represent the current density because of the additional induced electric field $\mathbf{v} \times \hat{\mathbf{y}}$.

The Hartmann layer can be omitted in the numerical model by integrating the equations analytically across the thin Hartmann layer.[5] As a result, the wall conductance ratio c_w at the Hartmann wall must be replaced by $c_w + \delta_H$, where $\delta_H = M^{-1}$ is the total conductance of the fluid layer. The physical model behind this substitution is that the wall and the layer are considered as electrical resistances connected in parallel. Equation (17) is a Poisson equation where the source term is the normal gradient of ϕ at the wall. To solve this equation, a direct Poisson solver was written. It gives the value of the potential in the plane of the wall. This value is then used as a Dirichlet boundary condition for the fluid domain. As already noticed[6] in the case of forced MHD convection, within the global iterative procedure, the errors in evaluating potential derivatives at the wall are amplified by a factor of $1/c_w$. Therefore, convergence is more difficult to obtain for the lowest values of the wall conductance ratio c_w. Convergence is achieved by a time-marching coupling between the electrical boundary condition Eq. (17) at the wall and the solution for ϕ in the fluid.

At the Hartmann walls, a reasonable condition for the tangential components of velocity, is the linear extrapolation from the values inside the domain.[8]

A more efficient way to treat the electrical boundary conditions is to use only the internal solvers available within the CFX code itself for heat and fluid dynamics. This is actually possible by modeling the conducting wall as a solid domain of finite thickness t rather than as an infinitely thin sheet. Then, it becomes possible to use the CFX heat transfer procedure to solve for the electrical potential. With this approach, the correct boundary conditions are of zero flux on the external faces of the solid walls. This ensures the global conservation of charge. Note that the convective terms in Eq. (12) do not apply to the solid regions and that stationary solutions are independent of $\bar{c}_p$ and $\bar{\rho}$ at the wall. Setting properties for the solid walls as $\bar{\lambda}_{side\text{-}wall} = c_w/t$, $\bar{\lambda}_{Hartmann\text{-}wall} = (c_w + M^{-1})/t$, the thin wall condition Eq. (17) is satisfied. This method is general as it applies to any geometry described by body-fitted coordinates. Thus, it can be used for practical MHD configurations and complex devices for which no specialized code is available. Then, one should take care to set the local physical properties for the solid wall according to the variable thickness of the Hartmann layer along the wall surface:

$$\bar{\lambda}_{Hartmann\text{-}wall} = \frac{(M\mathbf{n}\cdot\hat{\mathbf{y}})^{-1} + c_w}{t} \quad , \tag{18}$$

where $\mathbf{n}$ is the normal unity vector to the wall and $\delta_H = (M\mathbf{n}\cdot\hat{\mathbf{y}})^{-1}$ is the local thickness of the layer. The case of fully developed MHD duct flow of arbitrary cross section with conducting walls in a magnetic field orthogonal to the axis has been studied for the first time by Chang and Lundgren.[9] It has been shown that the application of Eq. (18) to various geometries leads to reasonable results.[10] This approach fails only close to the points where the boundaries are tangent to the magnetic field direction, where some special criterion should be adopted to limit the value of the effective wall conductivity. Roberts[11] has shown that the error applying Eq. (18) is large only within a small radius of $O(M^{-1/3})$ around the tangential point in the surface and that it extends with a radius of $O(M^{-2/3})$ within the fluid. The error concerning the total flow rate is even smaller and does not contribute to the solution in the core at the leading order of approximation.

Note that in principle, it is possible to treat several sheets of conducting materials with different properties surrounding the fluid domain, or the case of perfectly conducting walls with an electrical resistance between the wall and the fluid. The latter configuration is known as the "insulating coating," and it has been studied, for example, by Bühler and Molokov.[12] All these cases can be dealt within CFX by choosing either Neumann or Dirichlet electrical boundary conditions at the external sides of the wall. Similarly, it is possible to model an infinite lattice of electrically coupled rectangular ducts by a set of periodic conditions along the $\hat{\mathbf{y}}$ and $\hat{\mathbf{z}}$ directions.

Our model can also be applied easily to pressure-driven MHD flow. In this case, the buoyancy term in the momentum equation Eq. (10) is just replaced by a constant forcing term. Once the flow field is known, the temperature distribution can be solved as an ordinary heat transfer problem. This approach is valuable for the design of self-cooled concepts in fusion reactors.

This second way to model electrical boundary conditions using internal solvers has proved to be much more efficient than the method described in the first part of the section; in particular, convergence speed is relatively high and only slightly influenced by the wall conductivity. There is no need of time-marching procedure or underrelaxation. About 5000 to 20 000 iterations are needed to get a converged solution. This is valid for the cases with internal heating, where the core currents are basically closed through the side layers and the side walls. The overall balance of the currents in this case is not very much affected by the Hartmann walls and layers. For the

differentially heated cases, convergence is difficult to obtain for $c_w \lesssim M^{-1}$, where the closure of the currents through the Hartmann walls and layers is crucial for a converged solution.

The cross section is resolved by a grid of $n_y \times n_z = 15 \times 250$ nodes for the calculations, with a nonequispaced distribution of the grid points along $\hat{\mathbf{z}}$. Because of the Hartmann layer model, the poor resolution along magnetic field lines is high enough to resolve all physical effects with sufficient accuracy. Periodic boundary conditions are imposed along the axis direction, and since fully developed flows are considered, only three grid points along the axis are sufficient to formulate the CFX model. For the simulations, a CRAY J90 version of CFX has been used.

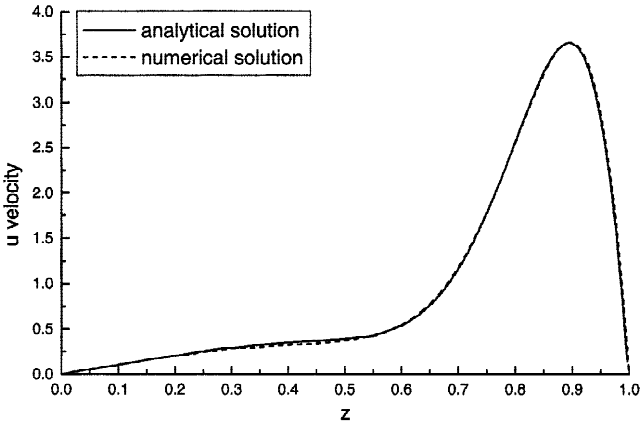

Fig. 3. Comparison between analytical and numerical solutions, in the plane $y = 0$, for a differentially heated duct, with $T = z$, $M = 100$, and perfectly conducting walls. In this case, the asymptotic theory applies almost exactly.

IV. RESULTS AND DISCUSSION

IV.A. Differentially Heated Duct

Let us first consider a differential heating across the side layers, choosing for example $T = -1$ and $+1$ as boundary values. From Eq. (7), the temperature profile is simply $T = z$ if no internal heat generation is present. Without Lorentz forces, the velocity profile would be a third-order polynomial with maxima of $\pm M^2/16$. With Lorentz forces, this profile is flattened. Figure 2 shows the velocity field for $M = 100$ and perfectly conducting walls ($c_w \to \infty$), where the damping effect becomes clear as the currents are at their highest. Figure 3 shows a comparison between the analytical and numerical solution in the plane $y = 0$ for the same set of parameters for which the asymptotic theory applies almost exactly.

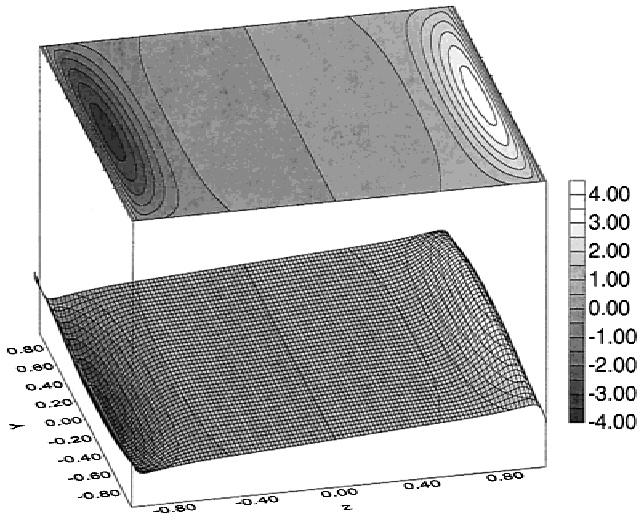

Fig. 2. Two-dimensional velocity distribution for a differentially heated duct with $T = z$, $M = 100$, and perfectly conducting walls. The flow exhibits velocity peaks in the side layers.

As the agreement between the theory and the computations is very good, our CFX model proves to be highly accurate. The velocity exhibits a linear profile in the core, where buoyancy is mainly balanced by Lorentz forces, the viscous effects being negligible in this region. The slope is near unity as found both by the theory and the numerical experiment. The main feature in the profile of the side layer is the presence of a high-velocity jet that is governed by the balance between the potential gradient and the induced electric field. Such a jet is also found in the asymptotic theory; the correction to the core solution in the side layer is $u \sim \partial_z \phi_s$, where ϕ_s is an additional contribution of the side layer potential to the core solution. Therefore, the flow rate carried by the layer is $\dot{m} \sim \int \partial_z \phi_s \, dz \sim (\phi_{core} - \phi_{side\text{-}wall}) \sim O(1)$. As already mentioned, the thickness of the side layer is $O(M^{-1/2})$, and thus, the velocity in the jet scales as $\sqrt{M}$ and is sustained by the gradient of potential, as shown in Fig. 4.

Figure 5 shows the velocity profiles in the plane $y = 0$ for some other values of the wall conductivity and $M = 100$. The case of perfectly insulating walls is also included. For the lower values of c_w, the MHD damping effect is less evident, but the solution in the core is still dominated by Lorentz forces, as one can see from the linear behavior. In the case of insulating walls, the slope is proportional to M, as in analytical solutions.[13,14] No jets are present in these cases. In fact, the core solution is simply corrected by viscous dissipation in the side layer so that the no-slip condition at the wall is satisfied. This behavior at the lower values of wall conductivity can be understood if we look at the currents normal to the walls shown in Fig. 6. Here, the coordinate ζ_{wall} starts from $y = 0$, $z = -1$ and follows the walls. For the highest value

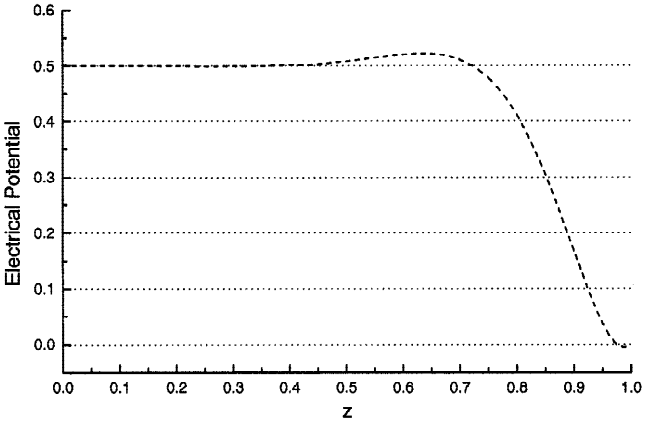

Fig. 4. Potential distribution, in the plane $y = 0$, for a differentially heated duct, with $T = z$, $M = 100$, and perfectly conducting walls. The velocity jet in the side layer is actually sustained by the potential gradient.

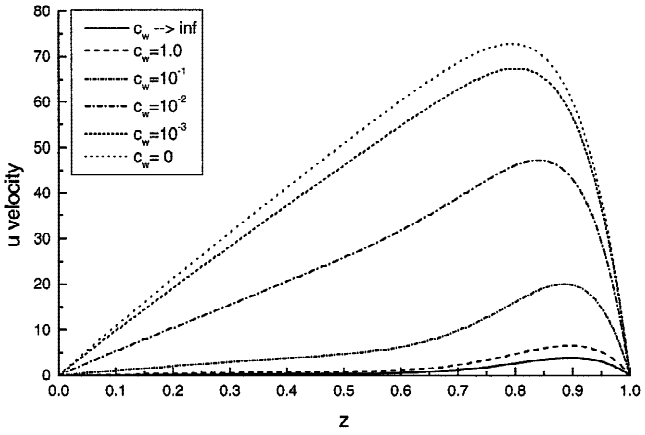

Fig. 5. Velocity profiles, in the plane $y = 0$, for a differentially heated duct, with $T = z$ and $M = 100$ for several values of the wall conductivity. For the limiting case of perfectly insulating walls and for the lower values of c_w, the velocity jets are not present, and the linear core solution is corrected in the side layer only by viscosity.

of c_w shown in the figure, the currents leaving the side walls pass almost unchanged through the side layers and close through the Hartmann wall and layer. For the lower values, the currents leaving the side wall are progressively reducing and are almost negligible for $c_w \lesssim 10^{-2}$. In these latter cases, the side layers become more conducting than the side walls, and high-current jets are now present in the layers, parallel to the side walls. Currents parallel to **B** do not interact with the magnetic field. Therefore, the electromagnetic forces in the side layers become small, and viscous dissipation is dominant. Of course, this behavior cannot be recovered by the asymptotic approach,[3] which is valid for highly conducting side

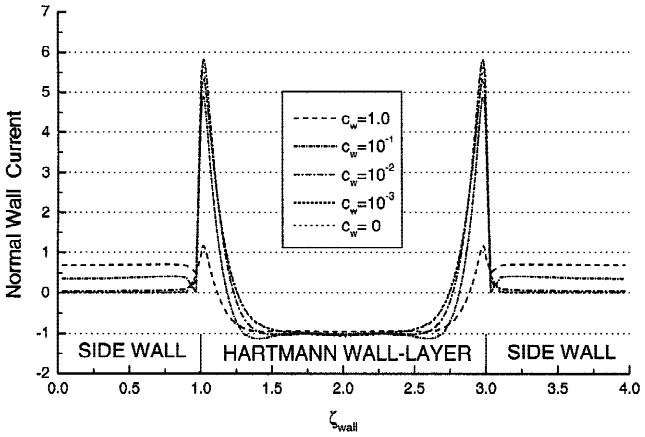

Fig. 6. Normal wall currents for a differentially heated duct, with $T = z$ and $M = 100$ for several values of the wall conductance ratio c_w. For walls that conduct well, currents leaving the side walls are basically totally closed via the Hartmann wall-layer. For walls that conduct weakly, the side layers become better conducting than the side walls, and high currents flow in the layers parallel to the walls before they enter the Hartmann walls near $\zeta_{wall} = 1$ or $\zeta_{wall} = 3$.

walls. Figure 7 shows the electrical potential distribution along the wall for some values of c_w and $M = 100$. From Ohm's law Eq. (5) and the thin wall condition Eq. (17), it appears that the first derivative of these distributions is proportional to the local currents within the wall as defined by the effective wall conductivity Eq. (18), while the second derivative is proportional to the currents

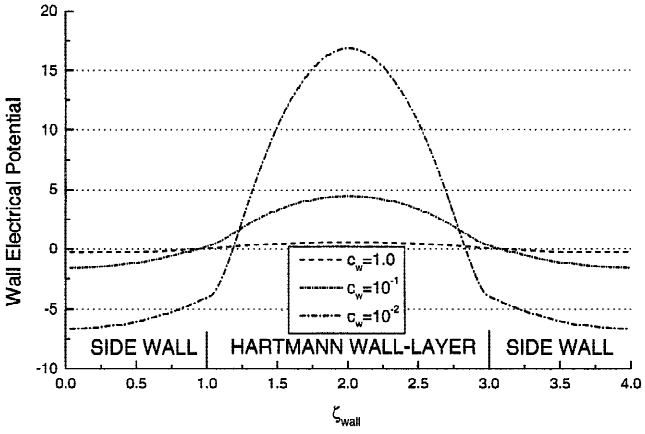

Fig. 7. Potential distribution for a differentially heated duct, with $T = z$ and $M = 100$ for some values of c_w. The first and the second derivatives, amplified by the local effective conductivity, give, respectively, the currents flowing within the walls, and the currents entering the walls normally.

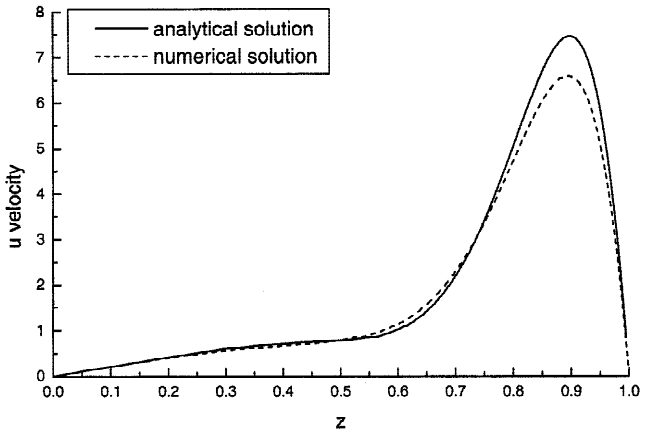

Fig. 8. Comparison between analytical and numerical solutions, in the plane $y = 0$, for a differentially heated duct, with $T = z$, $M = 100$, and $c_w = 1$. The agreement is quite good in the core, while in the side layer the asymptotic approach does not apply exactly because relevant currents flow parallel to the wall within the side layer.

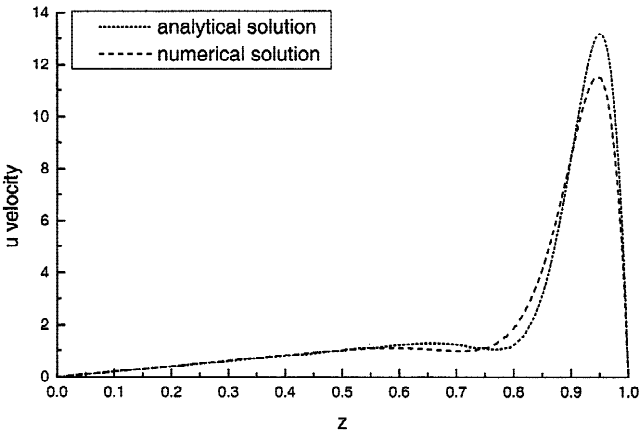

Fig. 9. Comparison between analytical and numerical solutions, in the plane $y = 0$, for a differentially heated duct, with $T = z$, $M = 400$, and $c_w = 1$.

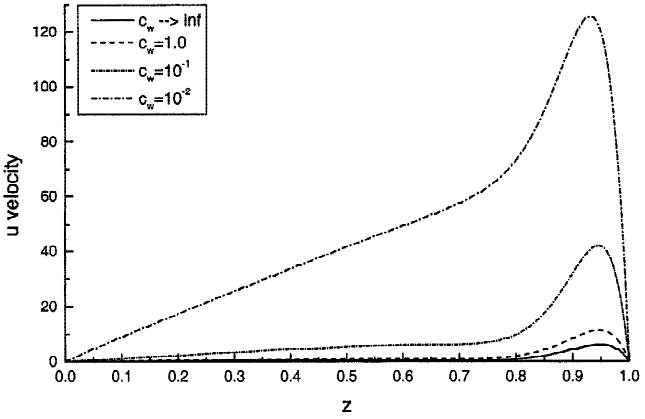

Fig. 10. Velocity profiles, in the plane $y = 0$, for a differentially heated duct, with $T = z$ and $M = 400$ for several values of the wall conductance ratio c_w. The limiting case of perfectly insulating walls is included.

entering the wall normally. Thus, for weakly conducting walls, the total currents flowing in the side walls are very low.

The agreement between the numerical and analytical results is also quite good for a relatively high conductivity of the wall. For $M = 100$ and $c_w = 1$, the criterion Eq. (9) is satisfied, but the actual thickness of the side layer seems to be larger than $M^{-1/2}$, and currents parallel to the walls are already significant.

Figure 8 shows such a comparison in the plane $y = 0$. The agreement is good in the core, while the maximum value is not correctly predicted by the theory. Similar remarks hold for higher values of the Hartmann number M, as shown in Fig. 9 for $M = 400$ and $c_w = 1$.

Figures 10 and 11 show velocity profiles for a differentially heated duct with $T = z$ and higher values of the Hartmann number, i.e., $M = 400$ and $M = 1000$. It should be noticed that for these relatively high values of M, the velocity profiles in the core are linear. This is valid also for the lower values of c_w and, as observed previously in this section, this states that the Lorentz electromagnetic forces still play a major role in the core of the fluid domain.

IV.B. Internally Heated Duct

If uniform internal heat generation is present, the temperature profile established is parabolic. Therefore, in the purely hydrodynamic case, the flow goes up in the center and down close to the left and right walls, which are kept at $T = 0$ if all other walls are adiabatic. To satisfy the condition of zero mass flux through the section, a dynamic compensative force in the momentum equation is needed to perform such simulations with internal heating. The hydrodynamic velocity profile in a plane case would be a fourth-order polynomial. The situation, of course, is very much modified by the presence of the magnetic field. The velocity profile is damped by Joule's dissipation, as shown in Fig. 12 for perfectly conducting walls, $M = 100$ and $Q = 1$ in the plane $y = 0$. High velocity jets are present again in the side layers, and the flow rate is O Eq. (1). Figure 13 shows results for several values of wall conductivity, $M = 100$ and $Q = 1$. As in the case of the differentially heated duct and for similar reasons, jets are suppressed as the conductivity of the wall decreases. In fact, the parabolic solution in the core is only corrected at the layers by viscous dissipation in order to satisfy the no-slip condition at the wall. The solution for $c_w = 10^{-3}$ is already very close to that of

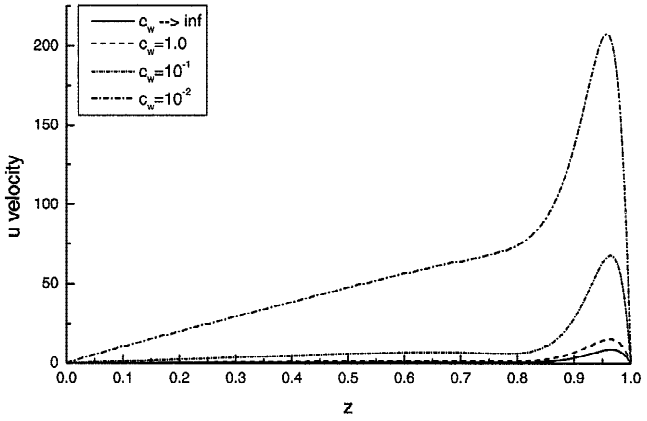

Fig. 11. Velocity profiles, in the plane $y = 0$, for a differentially heated duct, with $T = z$ and $M = 1000$ for several values of the wall conductance ratio c_w. The limiting case of perfectly insulating walls is included.

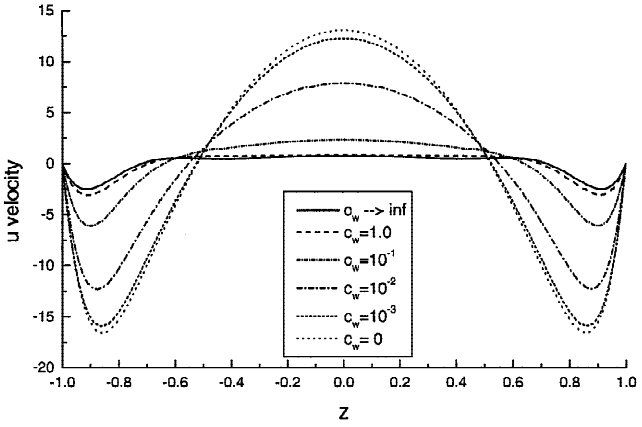

Fig. 13. Velocity distributions in the plane $y = 0$, for an internally heated duct, with $Q = 1$ and $M = 100$ for several values of the wall conductance ratio c_w. The limiting cases of perfectly conducting and perfectly insulating walls are included.

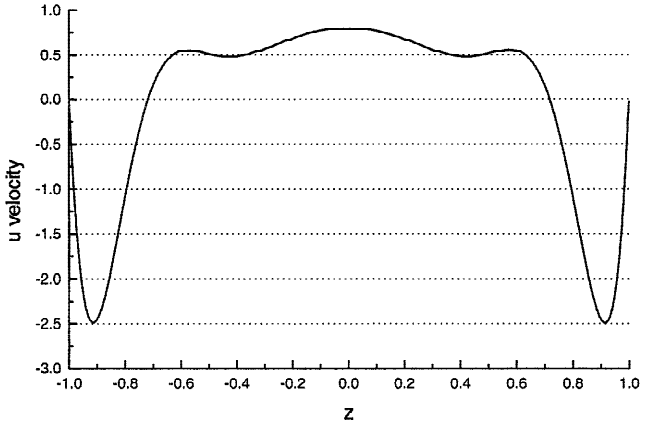

Fig. 12. Velocity distribution in the plane $y = 0$, for an internally heated duct, with $Q = 1$ and $M = 100$. The flow is strongly damped in the core, while high velocity jets occur in the layers.

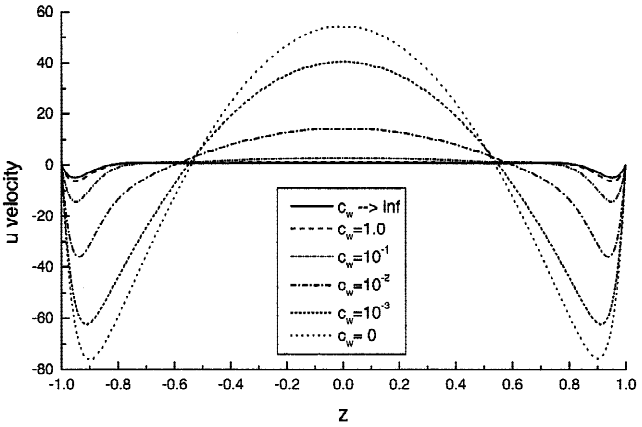

Fig. 14. Velocity distributions in the plane $y = 0$, for an internally heated duct, with $Q = 1$ and $M = 400$ for several values of the wall conductivity c_w.

perfectly insulating walls. This is not the case for higher values of the Hartmann number, as shown on Figs. 14 and 15, where the conductance of the layers is relatively low and a residual influence of the wall conductivity is still present above 10^{-3}. A comparison between solutions at different Hartmann numbers is given in Fig. 16 for $c_w = 1$. The core solution matches the numerical model in all cases, and the thickness of the side boundary layer decreases as M increases. This is shown better by Fig. 17, in which the side layer thickness δ_s is computed as the distance between the wall and the inflection points of the velocity jets in Fig. 16. The theoretical scaling of δ_s as $\delta_s \sim M^{-1/2}$ is fully confirmed by the computations, even for the relatively low Hartmann number $M = 100$. It must be pointed out that this result is a consequence of the solution of the basic flow equations, without any assumption on the thickness of the side layers. Similar remarks to those of the previous section hold for the currents and their role in the flow pattern. High currents occur in the layers for the low-conducting cases, as shown in Fig. 18 for $M = 1000$ and $Q = 1$.

V. CONCLUSIONS

Numerical simulations of MHD buoyancy-driven flow in a vertical square duct have been presented. The CFX package has been used for all the calculations. The proper description of an MHD problem within this code is discussed, with particular attention to the Lorentz

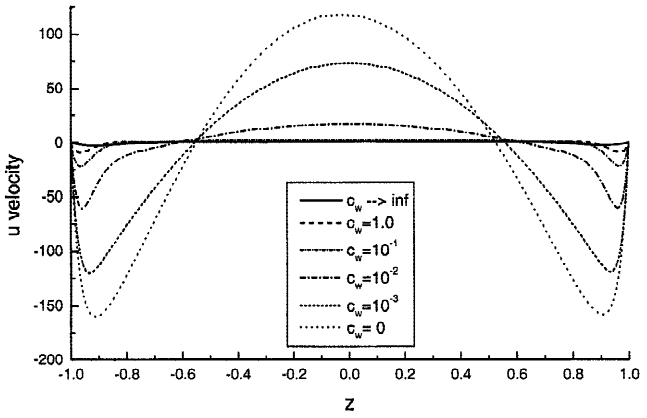

Fig. 15. Velocity distributions in the plane $y = 0$, for an internally heated duct, with $Q = 1$ and $M = 1000$ for several values of the wall conductance ratio c_w. For these higher Hartmann numbers, the solution obtained for $c_w = 10^{-3}$ is still far from the limiting case of perfectly insulating walls.

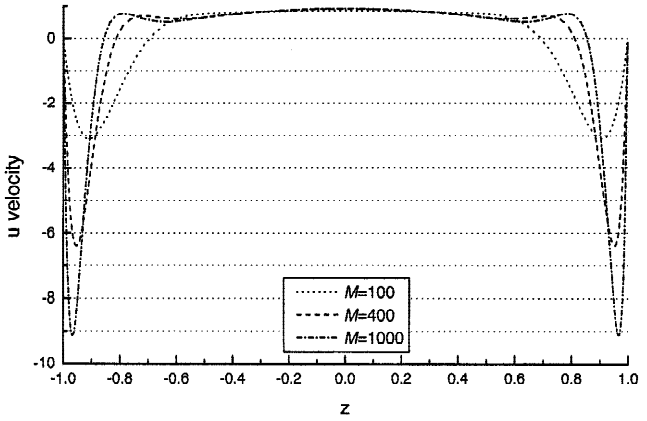

Fig. 16. Comparison between numerical solutions in the plane $y = 0$, for an internally heated duct, with $Q = 1$, $c_w = 1$, and three different values of the Hartmann number. The solution in the core is almost independent of M, while the thickness of the side layer scales as $\sim M^{-1/2}$.

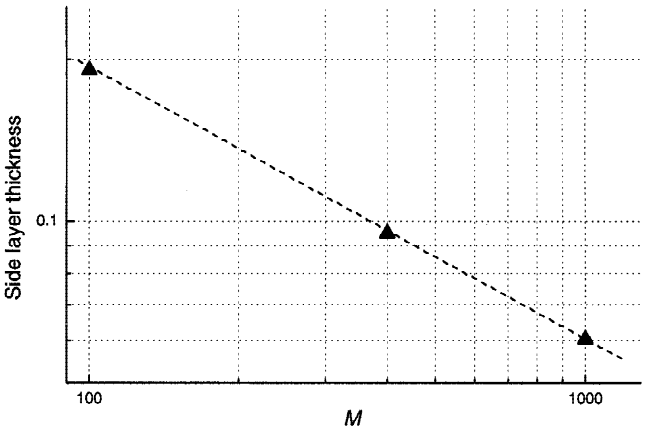

Fig. 17. Comparison between numerical solutions in the plane $y = 0$, for an internally heated duct, with $Q = 1$, $c_w = 1$, and three different values of the Hartmann number. The thickness of the side layer is computed as the distance of the velocity inflection point from the wall. This thickness scales almost perfectly as $\sim M^{-1/2}$.

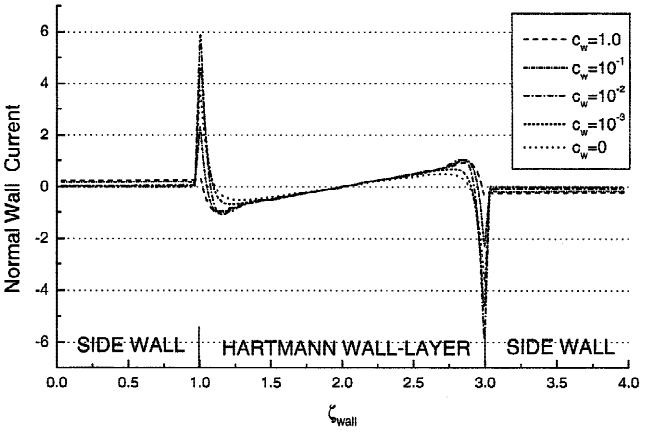

Fig. 18. Currents occurring normally at the walls in an internally heated duct, with $Q = 1$, $M = 1000$, and several values of c_w. As in the differentially heated duct, high currents flow in the side layers for the weakly conducting walls.

forces, the potential equation, and the electrical boundary conditions. The method presented is very general and allows us to treat practical configurations using body-fitted coordinates, with arbitrary electrical conductivity of the walls. Pressure-driven flows can also be computed. It is possible also to study flows in different domains that are electrically coupled or configurations with insulating coatings. Results in a wide range of wall conductivities are illustrated and compared with the asymptotic theory. The ability of CFX to describe accurately MHD phenomena has been shown by comparing numerical and analytical results in some asymptotic cases. The agreement is very good for walls that conduct well, and high velocity jets are correctly predicted in the side layer, while the numerical simulations at lower values of wall conductivity give high current density flowing in the layer parallel to the side wall. With such lower values of c_w, the layers are more conducting than the walls, and in the limit of insulating walls, the whole current closes through the side layers.

The MHD problem in CFX, in particular the equation for electric potential, is treated as an equivalent to a heat transfer problem in a medium at rest, using conducting solid walls in order to describe the electrical thin-wall boundary condition. This is an efficient way to solve the problem within the CFX package. Another method is in fact proposed to couple the CFX solvers for the fluid domain with an external Poisson solver, which provides a Dirichlet boundary condition for the electrical potential. With this latter method, the convergence speed is much lower and an iterative procedure must be adopted. Nevertheless, the coupling between the electrical potential and the velocity field is similar to the well-known pressure-velocity coupling. Therefore, it would probably be even more efficient to treat the electrical potential like a pressure using the same SIMPLE family algorithm for the velocity coupling but satisfying the thin-wall boundary conditions. This is not possible at the moment with CFX, because the SIMPLE algorithm is available only for the pressure, and a second variable similar to a pressure cannot be actually defined by the user.

REFERENCES

1. J. REINMANN, G. BENAMATI, and R. MOREAU, "MHD Issues of the European Self-Cooled and Water-Cooled 83Pb-17Li Blankets," *Proc. 19th Symp. Fusion Technology*, Lisbon, Portugal, September 16–20, 1997, p. 1527, C. VARANDAS and F. SERRA, Eds., North-Holland Publishing Company, Amsterdam, The Netherlands (1997).

2. "CFX-4.2: Solver," CFX-International (1997).

3. L. BÜHLER, "Laminar Buoyant Magnetohydrodynamic Flow in Vertical Rectangular Ducts," *Phys. Fluids*, **10**, 223 (1998).

4. H. BEN HADID and D. HENRI, "Numerical Study of Convection in a Horizontal Bridgeman Configuration Under the Action of a Constant Magnetic Field. Part 2: Three-Dimensional Flow," *J. Fluid Mech.*, **333**, 57 (1997).

5. B. MÜCK, "Numerische Untersuchung von Strömumgen in Kanälen mit Versperrungen unter dem Einfluß von Magnetfeldern," FZKA 6292, Forschungszentrum Karlsruhe (1998).

6. A. STERL, "Numerical Simulation of Liquid-Metal MHD Flows in Rectangular Ducts," *J. Fluid Mech.*, **216**, 161 (1990).

7. J. S. WALKER, "Magnetohydrodynamic Flows in Rectangular Ducts with Thin Conducting Walls," *J. Mec.*, **20**, 79 (1981).

8. L. LEBOUCHER, "Monotone Scheme and Boundary Conditions for Finite Volume Simulation of Magnetohydrodynamic Internal Flows at High Hartmann Number," *J. Comput. Phys.*, **150**, 181 (1999).

9. C. CHANG and S. LUNDGREN, "Duct Flow in Magnetohydrodynamics," *ZAMP*, **XII**, 100 (1961).

10. L. BÜHLER, "Magnetohydrodynamic Flows in Arbitrary Geometrics in Strong, Nonuniform Magnetic Fields—A Numerical Code for the Design of Fusion Reactor Blankets," *Fusion Technol.*, **27**, 3 (1994).

11. P. H. ROBERTS, "Singularities of Hartmann Layers," *R. Soc. London*, **300**, 94 (1967).

12. L. BÜHLER and S. MOLOKOV, "Magnetohydrodynamic Flows in Ducts with Insulating Coatings," *Magnetohydrodynamics*, **30**, 439 (1994).

13. S. ALEKSANDROVA, "Natural Convection in a Rectangular Cavity in a Strong Vertical Magnetic Field," Technical Report Transfer Document from MPhil/PhD to PhD, Coventry University M.I.S. (1999).

14. V. BOJAREVICS, "Buoyancy Driven Flow and Its Stability in a Horizontal Rectangular Channel with an Arbitrary Oriented Transverse Magnetic Field," *Proc. 2nd Int. Conf. Energy Transfer in Magnetohydrodynamic Flows*, Aussois, France, September 26–30, 1994, Vol. 1, p. 37 (1994).

Ivan Di Piazza is finishing his PhD in computational fluid dynamics at the University of Palermo, Italy. He has worked on natural convection phenomena in low-Prandtl number fluids and numerical simulations of heat exchangers of complex shape. At the Karlsruhe Forschungszentrum (FZK), for six months in 1999, he collaborated on the general implementation of magnetohydrodynamic (MHD) problems in the commercial package CFX-FLOW3D.

Leo Bühler (Dipl Ing, 1988, and Dr Ing, 1992, University of Karlsruhe, Germany) works at the Institute for Nuclear and Energy Technologies at FZK. His research activities are focused on fluid dynamics, thermal convection, solidification, and liquid-metal MHD flows and their applications in fusion blankets.